Formation of heterostructures with multiple quantum wells InN/InGaN by the PA-MBE method on sapphire

© M.A. Kalinnikov[1], D.N. Lobanov[1], K.E. Kudryavtsev[1], B.A. Andreev[1], P.A. Yunin[1], L.V. Krasilnikova[1], A.V. Novikov[1], E.V. Skorokhodov[1], Z.F. Krasilnik[1,2]

[1] Institute for Physics of Microstructures, Russian Academy of Sciences, 603087 Nizhny Novgorod, Russia
[2] Lobachevsky State University, 603950 Nizhny Novgorod, Russia

E-mail: kalinnikov@ipmras.ru

Received June 30, 2022
Revised July 7, 2022
Accepted July 7, 2022

The features of the process of growth of multilayer heterostructures with InN/InGaN quantum wells (QWs) by the method of molecular-beam epitaxy with nitrogen plasma activation in the mode of modulated metal fluxes are studied. To compensate for elastic stresses in the structure, the active region was formed in the form of an InN/InGaN superlattice matched over the average lattice parameter with the underlying InGaN buffer layer. It has been shown that during the growth of relatively narrow InN QWs up to 3 nm wide, there is no relaxation of elastic stresses in the active region of the structure, and the dislocation density remains at the level $N_D \sim (3-4) \cdot 10^{10}\,\mathrm{cm}^{-2}$, which corresponds to the dislocation density in InGaN-buffer. Such structures demonstrate the most intense PL in the wavelength range of $1.3-1.5\,\mu$m. With the growth of wider QWs, the imperfection of the structures sharply increases ($N_D > 10^{11}\,\mathrm{cm}^{-2}$), which is accompanied by a decrease in the emission intensity. The structures grown with InN/InGaN QWs demonstrated an order of magnitude better temperature stability of PL compared to bulk InN layers (PL quenching by ~ 3 and ~ 25 times, respectively, in the temperature range of $77-300\,\mathrm{K}$). Nevertheless, at a low temperature ($T = 77\,\mathrm{K}$), the PL intensity of the studied structures with InN/InGaN QWs is noticeably inferior to that for the bulk InN layer, which apparently indicates a significant role of nonradiative recombination by the Shockley–Reed–Hall mechanism in structures with QWs (as opposed to Auger recombination in bulk InN).

Keywords: indium and gallium nitride, molecular beam epitaxy, quantum well, photoluminescence, dislocations.

DOI: 10.21883/SC.2022.09.54126.38

1. Introduction

Indium nitride, its ternary solutions with gallium, and heterostructures based on InGaN are of interest as materials for the design of optoelectronic devices (specifically, near-infrared (near-IR) emitters). At a time when the technology of light-emitting diodes and lasers based on GaN and InGaN compounds with a small fraction of indium [1,2] is advancing rapidly, the progression of InGaN structures toward the IR region is hindered by the issues arising in growth of InN and InGaN with a high indium concentration. Key among them are the low ($\sim 500^\circ$C) decomposition temperature of the material [3] and high densities of defects and metallic inclusions [4], which translate into high a background density of free electrons [5]. At the same time, stimulated emission (SE) in a wavelength range of $1.1-1.9\,\mu$m [6,7] at temperatures up to $200-210\,\mathrm{K}$ was demonstrated even in structures with a fairly low degree of perfection (planar waveguide structures with an active InN or InGaN layer). The formation of low-dimensional InN/InGaN structures appears to be a natural route for development in this research field with a focus on raising the operating temperature and reducing the generation threshold. Among the already reported advancements are lasing achieved at $T = 300\,\mathrm{K}$ in the red spectral region in structures with InGaN quantum dots (QDs) formed on an n^+-GaN substrate [8] and a series of studies focused on dot-in-nanowire InN/InGaN structures (see, e.g., [9,10]).

Naturally, while offering lower densities of structural defects and higher temperature stabilities of emission properties, emitters based on dot-in-nanowire InN/InGaN structures also have certain drawbacks associated primarily with the smallness of the emitting volume and the complexity of fabrication of device structures (i.e., lasers, including various types of cavity structures based on photonic crystals) based on arrays of grown nanowire crystals. In this context, planar structures with InN/InGaN QWs could appear advantageous. However, studies focused on heterostructures with InN/InGaN or InGaN/InGaN QWs with a high In concentration needed for lasing in the near IR range are scarce at present [11–14]. This is largely attributable to the specifics of fabrication of narrow-band (with indium fraction [In] $> 40-50\%$) InGaN layers amid such factors as indium segregation, thermal decomposition of the growing layer, and its phase decay (see, e.g., [15]). At the same time, the specifics of growth of mismatched materials also need to be taken into account in the fabrication of heterostructures with InN/InGaN QWs: since the lattice parameters of

InN and GaN differ by 11%, considerable elastic stresses emerge in QWs even at a moderate (15−20%) gallium concentration in barrier InGaN layers. Thus, the potential for variation of both the width of InN QWs and the composition of barrier InGaN layers (and, consequently, the band discontinuity at the heteroboundary) is limited by the processes of plastic QW relaxation due to the formation of dislocations, which are efficient nonradiative recombination centers [16]. This complicates the process of selection of the optimum InN/InGaN QW parameters in terms of carrier localization. Note also that the current theoretical estimates of critical QW widths deviate greatly from the experimental data [12,13] and need to be updated. The presence of elastic stresses and, consequently, a built-in field in the structure also affects the process of radiative recombination of carriers in InN/InGaN QWs due to the Stark effect. Designs focused on improving the carrier localization in QWs by increasing the InN QW width or the height of InGaN barriers may turn out to be less efficient due precisely to the spatial separation of electrons and holes in QWs and the corresponding reduction in the probability of radiative recombination [2,17]. All the above factors need to be balanced precisely to achieve the highest possible radiative efficiency of heterostructures with InN/InGaN QWs.

In the present study, the process of growth of light-emitting structures with an active region in the form of an InN/InGaN superlattice (SL) by plasma-assisted molecular beam epitaxy (PAMBE) with modulation of metal fluxes (MME, metal modulated epitaxy) is examined. The indicated method stipulates a cyclic growth process with metal-enriched growth conditions at the first stage and exposure of the growth surface to a flux of active nitrogen at the second stage for fixation of accumulated excess metal [18,19]. It was demonstrated that such an approach, which allows one to fabricate both uniform InGaN layers and periodic InN/InGaN structures, may be efficient in reducing the density of threading dislocations, suppressing the effects of phase separation, and enhancing the surface morphology of the structures being formed [20–22]. The aim of the present study is to examine the dependence of structural and optical (emissive) properties of multilayer heterostructures with InN/InGaN QWs with the fraction of indium in barrier layers being $[\mathrm{In}] \sim 76-83\%$ on the QW width and identify the optimum QW width values that enable intense photoluminescence (PL) in the near IR range with the minimum thermal quenching.

2. Experimental procedure

The studied multilayer heterostructures with InN/InGaN QWs were grown by PAMBE using an STE 3N3 unit (ZAO „NTO“) and Al_2O_3 substrates with the [0001] orientation of the growth surface. The structure being formed consisted of sequentially deposited buffer AlN and GaN layers, a relaxed InGaN buffer, and an active region (InN/InGaN superlattice matched with the InGaN buffer in the period-average lattice parameter). AlN and GaN layers with thickness $d_{\mathrm{AlN}} \sim 200$ nm and $d_{\mathrm{GaN}} \sim 700$ nm were grown at high temperature $T_{\mathrm{gr}}^{\mathrm{AlN}} = 820^\circ\mathrm{C}$ and $T_{\mathrm{gr}}^{\mathrm{GaN}} = 710^\circ\mathrm{C}$. Both the InGaN buffer and the active region were grown at substantially lower temperatures ($T_{\mathrm{gr}} \sim 440-460^\circ\mathrm{C}$) in the regime of cyclic MME growth with modulation of the metal component fluxes. An RF Atom Source HD25 (Oxford Applied Research) was used as the source of atomic nitrogen; the nitrogen flux and the discharge power in the process of growth of the InGaN buffer and the InN/InGaN superlattice were fixed at 2 sccm (standard cubic centimeters per minute) and 130 W, respectively, and provided deposition rate $F_{\mathrm{N}} \sim 0.27\,\mu$m/h of active nitrogen (per lattice parameter of $In_{0.8}Ga_{0.2}N$). The indium flux in the process of growth of all structures was $F_{\mathrm{In}} \sim 0.28\,\mu$m/h, while the gallium flux was varied ($F_{\mathrm{Ga}} \sim 0.04-0.08\,\mu$m/h) depending on the target composition of the buffer and barrier InGaN layers. Thus, the ratio of fluxes of metals and active nitrogen III/V was $\sim (1.1-1.2)$. With this ratio, excess metal is accumulated on the growth surface at the first stage of MME growth.

In the process of growth of the buffer InGaN layer, the gate opening times were chosen so that < 1 metal monolayer (ML) accumulated on the growth surface. Indium segregation was not observed in this case, and a uniform epitaxial InGaN layer formed [20]. The fixation of excess metal at the second stage of the MME cycle (with the growth surface exposed to a flux of active nitrogen) was identified by examining the pattern of reflection high-energy electron diffraction (RHEED): band reflections, which are typical of an atomically smooth surface forming in the course of metal-enriched growth owing to an elevated mobility of adatoms [21], gave way to a bright $(\sqrt{3} \times \sqrt{3})$ surface reconstruction pattern typical of [0001] InGaN [22]. The buffer InGaN layer was fairly thick (~ 100 nm) in all the grown structures, thus providing for a complete relaxation of elastic stresses, which was confirmed by X-ray diffraction analysis data. This agrees with the available literature data on the degree of relaxation of InGaN layers of various composition and thickness grown on GaN [23].

The process of growth of the active region (InN/InGaN superlattice) differed from that of the InGaN buffer layer only in the gate opening times for metal fluxes, which were chosen so that 2 (or more) MLs of excess metal accumulated on the growth surface in each cycle. It is well-known that a periodic structure forms in such conditions in the direction of layer growth [20,24,25]. This is attributable to the fact that, owing to the difference in Ga−N and In−N binding energies, the probability of incorporation of Ga atoms into a growing InGaN layer is considerably higher than the corresponding probability for In atoms. Thus, the process of accumulation of material on the growth surface is dominated by indium, which serves to form InN QWs at a later stage when the growth surface is exposed to a nitrogen flux. Since the layer growth rate is set by a (constant) active nitrogen flux, the In fixation, which

Growth parameters and characteristics of the studied samples*

№ Sample	d_{QW}, nm	d_{barr}, nm	x_{In}^{barr}, %	x_{In}^{buf}, %	N_D, 10^{10} cm^{-2}	n_e, 10^{19} cm^{-3}
193	1	4.6	82	85	3.7	1.31
194	2	9	83	88	3.7	1.38
195	3	9.5	83	88	3.4	1.53
199	4	9.3	78	87	6.7	2.62
201	5.7	12.8	76	87	11	4.22

Note. * Indicated are the nominal QW thicknesses (d_{QW}) in the InN/InGaN SL being formed, the thicknesses and compositions of barrier layers (d_{barr} and x_{In}^{barr}), the indium fraction in the buffer InGaN layer (x_{In}^{buf}), the density of threading dislocations (N_D), and the density of free electrons (n_e) measured at $T = 300$ K.

is timed by the rearrangement of the RHEED pattern, allows one to determine the InN QW width. It should also be noted that synchronous blockage of In and Ga fluxes automatically matches the „average composition“ of the obtained InN/InGaN superlattice to the composition of the lower-lying buffer InGaN layer, and this translates into matching of „average“ lattice parameters. One may thus circumvent the accumulation of elastic stresses, which would inevitably lead to partial relaxation of structures and additional generation of mismatch dislocations, in a multiperiod SL. The indium gate was opened additionally at the second stage of the MME cycle in the process of growth of wide (> 2.5 nm) InN QWs to provide the needed amount of material. The element fluxes at the stages of formation of the InGaN buffer and the active region with InN/InGaN QWs were then adjusted accordingly to compensate for elastic stresses.

The fraction of indium in the studied series of samples varied within the range of $x_{In}^{buf} \sim 87-88\%$ in the intermediate InGaN buffer and as $x_{In}^{barr} \sim 76-83\%$ in barrier layers of the superlattice being formed. The width of InN QWs was $d_{InN} \sim 1-5$ nm at SL period $d_{SL} \sim 6-19$ nm; the net width of the InN/InGaN SL was ~ 450 nm in all samples. The parameters of the studied samples are listed in the table.

A structure with a bulk InN layer with a thickness of ~ 650 nm was prepared for reference. It was grown in nitrogen-enriched conditions (the III/V flux ratio was ~ 0.9) established by increasing the discharge power of the plasma nitrogen source to 140 W and, consequently, the deposition rate of active nitrogen to $\sim 0.33\,\mu$m/h). This nitrogen-enriched growth was chosen for the reference sample based on the understanding that InN layers formed under such conditions both demonstrate an intense spontaneous PL signal and allow for stimulated emission [26].

3. Results and discussion

X-ray diffraction (XRD) analysis, scanning electron microscopy (SEM), Hall measurements, and photoluminescence spectroscopy were performed to characterize the obtained structures with InN/InGaN QWs. The period of the formed InN/InGaN SL and its average composition were determined based on (0002) $\omega-2\Theta$ XRD spectra (Fig. 1). Marked higher-order satellite peaks are indictive of a fine periodicity of the structure. Data on the average composition of the InN/InGaN SL provide an opportunity to verify the InN QW widths determined based on the calibration of fluxes of deposited elements and the time of alteration of the RHEED pattern on exposure of the growth surface to a nitrogen flux in the MME cycle.

The density of threading dislocations (see N_D in the table) in the obtained structures was derived from the width of diffraction peaks, which were recorded by scanning in the (0004) and (10$\bar{1}$2) directions, in accordance with the procedure outlined in [27]. The value of N_D for sufficiently narrow InN QWs (with a width up to 3 nm) was $(3-4) \cdot 10^{10}$ cm^{-2}, and the defect density was largely the same as the one in the buffer InGaN layer (see, e.g., the data from [20]). At the same time, structures with wider QWs demonstrate considerably higher dislocation densities ($\sim 10^{11}$ cm^{-2} at $d_{QW} = 5.7$ nm), which are indicative of the engagement of plastic relaxation of elastic stresses in the SL by generation of mismatch dislocations. All the studied samples are, according to SEM data, have the form of continuous two-dimensional layers with their surface roughness decreasing with increasing InN QW width (Fig. 2).

The latter fact is attributable to the accumulation of a greater amount of excess indium, which is needed to form a wide InN QW, on the growth surface at the first stage of the MME cycle. Thus, the balance of fluxes in deposition of sufficiently thick barrier InGaN layers shifts effectively toward metal-enriched growth, which facilitates smoothing of the growth surface [28].

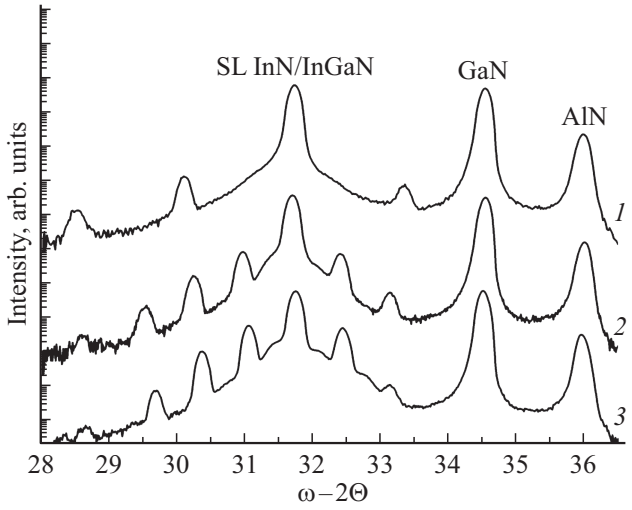

Figure 1. (0002) $\omega-2\Theta$ X-ray diffraction spectra for structures with MQWs InN/InGaN: *1* — sample № 193 ($d_{QW} = 1$ nm; see the table), *2* — № 195 ($d_{QW} = 3$ nm), *3* — № 199 ($d_{QW} = 4$ nm). The peaks denoted as GaN and AlN are related to the corresponding buffer layers.

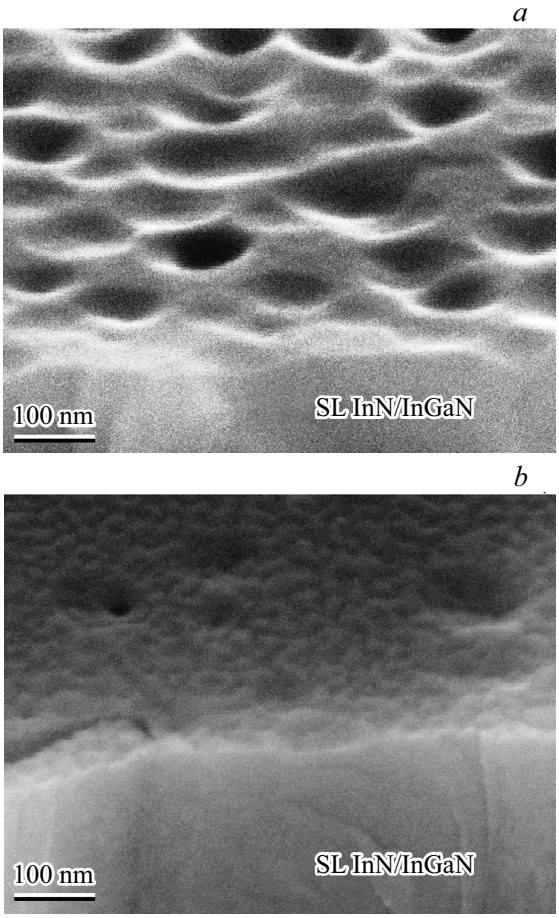

Figure 2. SEM images of the surface and the transverse cleavage of samples № 193, $d_{QW} = 1$ nm (a) and № 195, $d_{QW} = 3$ nm (b).

Hall measurements in the Van der Pauw geometry were performed to determine the density of free electrons in the grown structures. The obtained results revealed that all samples are characterized by a high (at the level of 10^{19} cm^{-3}) background electron density. The lowest values were $n_e \sim (1.3-1.5) \cdot 10^{19}$ cm^{-3} in samples with QWs with a width up to 3 nm, while the samples with wider QWs had n_e in excess of $2 \cdot 10^{19}$ cm^{-3}. The observed n_e enhancement at higher QW width values may be related both to an increase in the density of threading dislocations, which are involved in the formation of donor centers in InN layers [29,30], and to the above-mentioned metal-enriched growth of barrier InGaN layers, which leads to an increase in the density of intrinsic (i.e., not associated with dislocations) electrically active defects [26].

The spontaneous PL spectra of the studied structures were measured at the temperatures of 77 and 300 K under weak excitation (up to 5 W/cm^2) with continuous pumping by a laser with a wavelength of 808 nm. Secondary emission was collected from the sample surface and analyzed using a grid monochromator fitted with a multi-element InGaAs photodetector with a cutoff wavelength of 2.1 μm. A single broad peak was detected in the emission spectra of all samples with InN/InGaN QWs (Fig. 3). It appears natural to attribute the observed shift of this peak toward lower energies in the samples with wider QWs to a reduction in the characteristic size quantization energy in wider QWs. The samples with relatively narrow (1–2 nm) QWs demonstrated the brightest PL; the PL intensity reduction in wider QWs may be induced by variations of the rate of both radiative and nonradiative processes.

The former factor is contingent on the differences in the characteristic scale of spatial separation of electrons and holes due to the Stark effect and, consequently, in the overlap of their wavefunctions. The second factor is governed by increases in the density of threading dislocations and the background electron density, which may affect the nonradiative recombination rate via the Shockley–Read–Hall and Auger mechanisms, respectively.

The available amount of experimental data is insufficient to examine in detail the relaxation processes in the studied InN/InGaN QWs. At the same time, it should be noted that the absolute PL intensity of structures with QWs at $T = 77$ K is significantly (almost 2 orders of magnitude) lower than the PL intensity of the reference sample (bulk InN layer). This is reflective of the difference in the ratio of rates of radiative and nonradiative processes in structures with QWs and bulk layers. The reduction in wavefunction overlap upon carrier separation due to the quantum-confined Stark effect, which was examined in relation to III-nitride structures with MQWs in [31], may be identified as one of the reasons behind the drop in emission intensity. This also affects the positioning of the PL line (see Fig. 3); specifically, since the energy of transitions in the PL spectrum of the structure with 4-nm QWs (sample № 199) does not exceed the energy of transitions in the bulk InN layer, the Stark effect in such QWs overcompensates the size quantization effect. At the same time, the observed shift in the balance of interband processes in favor of nonradiative recombination can hardly be attributed exclusively to the suppression of radiative recombination due to charge separation in QW structures. First, the overlap of wavefunctions of electrons and holes remains significant in relatively narrow ($d_{QW} = 1-3$ nm) QWs: according to the results of simulations based on a self-consistent solution of the Schrödinger and Poisson equations in the ATLAS module of SILVACO TCAD (the band structure of InN/InGaN QWs was calculated in accordance with [32] within the three-band $k-p$ model for deformed wurtzite with spontaneous and piezoelectric polarization taken into account), this overlap is ~ 0.57 at $d_{QW} = 1$ nm and ~ 0.38 at $d_{QW} = 3$ nm. Second, and more importantly, the same wavefunction overlap affects directly the efficiency of Auger recombination, which is an interband relaxation mechanism that is dominant in bulk InN (InGaN) layers at electron densities upward of 10^{19} cm^{-3} [33]. Thus, the resultant lifetime of excess carriers in QWs with no competing relaxation processes should increase relative to the one in bulk InN layers. This effect was observed, e.g., in [14], but we did not notice any appreciable extension of the

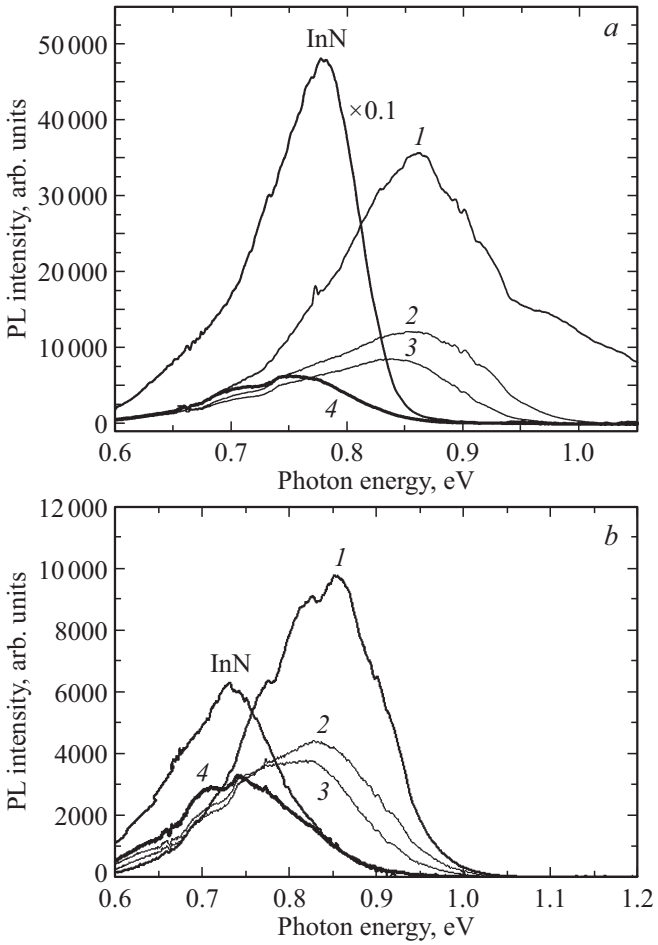

Figure 3. Spontaneous PL spectra of samples with InN/InGaN MQWs measured at temperatures $T = 77$ (*a*) and 300 K (*b*) under weak continuous pumping by a laser with a wavelength of 808 nm: *1* — sample № 193 (1-nm QWs), *2* — № 194 (2-nm QWs), *3* — № 195 (3-nm QWs), *4* — № 199 (4-nm QWs); InN — reference sample with a bulk layer.

PL decay kinetics in structures with InN/InGaN QWs in our experiments (the measured PL decay times did not exceed 100–150 ps; these measurements were limited by the temporal resolution of the detection system). This implies that recombination channels other than radiative and Auger recombination (and significantly faster than these two channels) should be present in the studied structures with InN/InGaN QWs. The possible options here are Shockley–Read–Hall recombination or the Auger mechanism involving defect-impurity centers. The difference in patterns of thermal PL quenching (while the PL intensity of the InN layer decreases by a factor of ~ 25 as the temperature increases from 77 to 300 K, the PL intensity of the structure with InN/InGaN QWs drops only by a factor of 3–5 in the same temperature interval) may also be attributed to the influence of different dominant mechanisms of interband relaxation. Note that similar data on PL quenching for InN and InN/InGaN QWs were reported in [14], but the thermal stability of PL of structures with QWs and their higher emissivity were attributed to a fine spatial localization of carriers. It should be noted here that the QW designs in the present study provide a carrier localization pattern generally consistent with the data from [14], and the observed differences in the relative PL intensity (compared to bulk InN) may be induced by the difference in the defect structure of heteroboundaries. It is not implausible that cyclic MME growth is more sensitive to the accumulation of point defects in the course of QW formation; nonradiative processes (Shockley–Read recombination) directly within QWs are intensified as a result and negate the positive influence of enhanced carrier localization in low-dimensional heterostructures.

4. Conclusion

Thus, heterostructures with multiple InN/InGaN QWs were grown by PAMBE with modulation of metal fluxes. It was found in the examination of such structures grown on an InGaN buffer layer with an indium concentration of $\sim 87\%$ that the critical width of InN QWs in an InN/InGaN superlattice matched with the buffer layer in the average period is ~ 3 nm. When this value is exceeded, plastic relaxation of elastic stresses in QWs commences, and the dislocation density increases sharply. Samples with narrow (1–2 nm) InN QWs demonstrate the highest PL intensity. This may be attributed to their lower degree of imperfection (in terms of both the dislocation density and the background density of free electrons) and a greater overlap of wavefunctions of electrons and holes (compared to wide QWs with a more pronounced Stark effect). The obtained structures with InN/InGaN QWs are characterized by a high thermal stability of photoluminescence (its intensity decreases by a factor of 3–5 as the temperature increases from 77 to 300 K, while the corresponding factor for a bulk InN layer is ~ 25). At the same time, the absolute PL intensity of structures with QWs at low temperatures is considerably lower than the one of the reference sample (bulk InN layer). This fact and the ultrashort (< 100 ps) lifetimes of inequilibrium carriers suggest that defect-impurity Shockley–Read–Hall recombination is the primary interband recombination channel in the studied InN/InGaN MQWs. This distinguishes them from bulk InN and InGaN layers, where Auger processes are dominant at the same densities of free electrons (on the order of 10^{19} cm^{-3}).

Funding

This study was carried out using USU „Femtospectrum“ at the common use center of the Institute for Physics of Microstructures of the Russian Academy of Sciences and was supported by the Russian Science Foundation (grant No. 22-22-00630).

Conflict of interest

The authors declare that they have no conflict of interest.

References

[1] Z.C. Feng. *Handbook of solid-state lighting and LEDs* (Boca Raton, FL, CRC Press, Taylor & Francis Group, 2017).
[2] T.D. Veal, C.F. McConville, W.J. Schaff. *Indium nitride and related alloys* (Boca Raton, FL, CRC Press, Taylor & Francis Group, 2011).
[3] Q. Guo, O. Kato, A. Yoshida. J. Appl. Phys., **73**, 7969 (1993).
[4] S.V. Ivanov, T.V. Shubina, T.A. Komissarova, V.N. Jmerik. J. Cryst. Growth, **403**, 83 (2014).
[5] H. Lu, W.J. Schaff, L.F. Eastman, J. Wu, W. Walukiewicz, D.C. Look, R.J. Molnar. MRS Symp. Proc., **743**, L4.10.1 (2003).
[6] B.A. Andreev, K.E. Kudryavtsev, A.N. Yablonskiy, D.N. Lobanov, P.A. Bushuykin, L. V. Krasilnikova, E.V. Skorokhodov, P.A. Yunin, A.V. Novikov, V.Yu. Davydov, Z.F. Krasilnik. Sci. Rep., **8**, 9454 (2018).
[7] D.N. Lobanov, K.E. Kudryavtsev, M.I. Kalinnikov, L.V. Krasilnikova, P.A. Yunin, E.V. Skorokhodov, M.V. Shaleev, A.V. Novikov, B.A. Andreev, Z.F. Krasilnik. Appl. Phys. Lett., **118**, 151902 (2021).
[8] T. Frost, A. Banerjee, K. Sun, S.L. Chuang, P. Bhattacharya. IEEE J. Quant. Electron., 49(11), 923 (2013).
[9] T. Frost, G.-L. Su, A. Hazari, J.M. Dallesasse, P. Bhattacharya. IEEE J. Select. Top. Quant. Electron., **23** (6), 1901409 (2017).
[10] P. Bhattacharya, A. Hazari, S. Jahangir. Proc. SPIE, **10553**, 1055302 (2018).
[11] B. Samuel, D. Cooper, N. Rochat, A. Mavel, F. Barbier, A. Dussaigne. J. Appl. Phys., **129**, 173105 (2021).
[12] S. Che, Y. Ishitani, A. Yoshikawa. Phys. Status Solidi C, **3** (6), 1953 (2006).
[13] T. Ohashi, P. Holmström, A. Kikuchi, K. Kishino. Appl. Phys. Lett., **89**, 041907 (2006).
[14] S. Valdueza-Felip, L. Rigutti, F.B. Naranjo, P. Ruterana, J. Mangeney, F.H. Julien, M. Gonzalez-Herraez, E. Monroy. Appl. Phys. Lett., **101**, 062109 (2012).
[15] G.B. Stringfellow. J. Cryst. Growth, **312**, 735 (2010).
[16] Q. Dai, M.F. Schubert, M.H. Kim, J.K. Kim, E.F. Schubert, D.D. Koleske, M.H. Crawford, S.R. Lee, A.J. Fischer, G. Thaler, M.A. Banas. Appl. Phys. Lett., **94**, 111109 (2009).
[17] O. Ambacher. J. Phys. D: Appl. Phys., **31**, 2653 (1998).
[18] S.D. Burnham, W.A. Doolittle. J. Vac. Sci. Technol. B, **24**, 2100 (2006).
[19] M. Moseley, J. Lowder, D. Billingsley, W.A. Doolittle. Appl. Phys. Lett., **97**, 191902 (2010).
[20] B.A. Andreev, D.N. Lobanov, L.V. Krasil'nikova, K.E. Kudryavtsev, A.V. Novikov, P.A. Yunin, M.A. Kalinnikov, E.V. Skorokhodov, M.V. Shaleev, Z.F. Krasil'nik. Fiz. Tekh. Poluprovodn., **55** (9), 766 (2021) (in Russian).
[21] E.J. Tarsa, B. Heying, X.H. Wu, P. Fini, S.P. den Baars, J.S. Speck. J. Appl. Phys., **82**, 5472 (1997).
[22] K. Hestroffer, F. Wu, H. Li, C. Lund, S. Keller, J. Speck, U.K. Mishra. Semicond. Sci. Technol., **30**, 105015 (2015).
[23] C.A.M. Fabien, B.P. Gunning, W.A. Doolittle, A.M. Fischer, Y.O. Wei, H. Xie, F.A. Ponce. J. Cryst. Growth, **425**, 115 (2015).
[24] E.A. Clinton, E. Vadiee, C.A.M. Fabien, M.W. Moseley, B.P. Gunning, W.A. Doolittle, A.M. Fischer, Y.O. Wei, H. Xie, F.A. Ponce. Solid-State Electron., **136**, 3 (2017).
[25] Z. Xing, W. Yang, Z. Yuan, X. Li, Y. Wu, J. Long, S. Jin, Y. Zhao, T. Liu, L. Bian, S. Lu, M. Luo. J. Cryst. Growth, **516**, 57 (2019).
[26] B.A. Andreev, D.N. Lobanov, L.V. Krasil'nikova, P.A. Bushuykin, A.N. Yablonskiy, A.V. Novikov, V.Yu. Davydov, P.A. Yunin, M.I. Kalinnikov, E.V. Skorohodov, Z.F. Krasil'nik. Semiconductors, **53** (10), 1357 (2019).
[27] M.A. Moram, M.E. Vickers. Rep. Progr. Phys., **72**, 036502 (2009).
[28] G. Koblmuller, S. Fernandez-Garrido, E. Calleja, J.S. Speck. Appl. Phys. Lett., **91**, 161904 (2007).
[29] L.F.J. Piper, T.D. Veal, C.F. McConville, L. Hai, W.J. Schaff. Appl. Phys. Lett., **88**, 252109 (2006).
[30] X. Wang, S.-B. Che, Y. Ishitani, A. Yoshikawa. Appl. Phys. Lett., **90**, 151901 (2007).
[31] M. Strassburg, A. Hoffmann, J. Holst, J. Christen, T. Riemann, F. Bertram, P. Fischer. Phys. Status Solidi C, **0** (6), 1835 (2003).
[32] S.L. Chuang. IEEE J. Quant. Electron., **32** (10), 1791 (1996).
[33] A. McAllister, D. Bayerl, E. Kioupakis. Appl. Phys. Lett., **112**, 251108 (2018).